Biol. Cybern. 88, 293–301 (2003)
DOI 10.1007/s00422-002-0382-6

Biological Cybernetics

Stability of bipedal stance: the contribution of cocontraction and spindle feedback

A. J. "Knoek" van Soest, Wouter P. Haenen, Leonard A. Rozendaal

Faculty of Human Movement Sciences and Institute of Fundamental and Clinical Human Movement Sciences, Free University, van der Boechorststraat 9, 1081 BT Amsterdam, The Netherlands

Received: 10 October 2002 / Accepted: 3 December 2002 / Published online: 3 April 2003

Abstract. The aim of this study is to assess the contribution of cocontraction and spindle feedback to local stability during bipedal stance. To that aim, an existing nonlinear state space model of the human musculoskeletal system is linearized in a reference equilibrium state. The maximal real part of the eigenvalues of the linearized system matrix A and the low-frequency joint stiffness are used as a measure of local stability. Muscle properties, as represented in a Hill-type muscle model, are shown to improve the behavior, the improvement being larger at high cocontraction. However, even at maximal cocontraction the low-frequency joint stiffness generated by the muscle properties is insufficient to yield a locally stable system. It follows that feedback is necessary to ensure local stability. In this study, the potential contribution of spindle feedback is investigated by optimizing the feedback gains for contractile element length and velocity for each muscle. It is found that in the case of time-delayed negative feedback, it is impossible to stabilize the system on the basis of spindle feedback. When positive time-delayed feedback is allowed, a barely stable system is obtained. When the time delays are removed, the feedback gains can be chosen such that a locally stable system is obtained, indicating the limitations imposed by the presence of time delays. Finally, it is shown that for small perturbations the response of the linear system to an arbitrary perturbation is similar to that of the nonlinear system, indicating the validity of the approach used. It is concluded that the combination of muscle properties and time-delayed spindle feedback is insufficient to obtain a system with reasonable local stability.

1 Introduction

Stable bipedal stance is not only an important task in itself, it is also an important prerequisite for execution of tasks involving both upper extremities. As the gravitational force destabilizes the inverted-pendulum-like skeletal system during bipedal stance, ensuring stability is an important task of the postural control system. The performance of the human postural control system has been evaluated in several different ways. Experimentally, human bipedal stance has most often been investigated in terms of the center of pressure (COP) trajectories, either during unperturbed stance (e.g., Collins and De Luca 1993) or after platform perturbations (e.g., Nakata and Kyonosuke 2001). In some studies, a measure of system stability is based on statistical quantities such as the root mean square of the COP trajectory (e.g., Nakata and Kyonosuke 2001). In other studies, stabilogram diffusion analysis (e.g., Collins and De Luca 1993) is employed, with the advantage that no assumptions are needed regarding the stationarity of the COP signal. Whatever the method used, it is not easy to characterize the stability of the high-dimensional neuromusculoskeletal system in terms of descriptors of the low-dimensional COP trajectory.

Phenomenological models have been proposed that reproduce the behavior of the COP both during unperturbed human stance and after platform perturbations. An example is the pinned polymer model (Chow and Collins 1995) that was later extended by Dijkstra (2000) with an extra degree of freedom representing the dynamic drift of the COP set point. Although the pinned polymer model is based on spontaneous postural sway data, Lauk et al. found that postural system dynamics are the same for quiet standing and small perturbations (Lauk et al. 1998; Chow et al. 1999). They concluded that this follows from the fact that at a certain time the postural system cannot distinguish between a random and applied perturbation, which suggests that the same neuromuscular control mechanisms are used under quiet-standing and dynamic conditions. Rosenblum et al. (1998) described the behavior of the COP with two coupled chaotic oscillators. Inverted-pendulum models have also been shown to be capable of reproducing experimental sway data (Eurich and Milton 1996; Peterka 2000).

Correspondence to: A. J. van Soest
(e-mail: a_j_van_soest@fbw.vu.nl)

Finally, structural models based on current knowledge of the dynamics of the neuromusculoskeletal system have been proposed (e.g., He et al. 1991; Kuo 1995; van der Kooij 1999). If simulation results from such models are in accordance with experimental data, such models can provide insight into the relative importance of the sources of sensory information. Most of the structural models proposed use high-level optimal control theory and assume a high-level controller that has full state information. Thus, these models do not take into account the hierarchical organization (e.g., Bernstein 1967) of the nervous system. In fact, it has been argued (van Soest and Bobbert 1993; Loeb et al. 1999) that the control problem for the higher parts of the central nervous system is overestimated when low-level contributions to system behavior, such as the viscoelastic properties that arise from the force-length-velocity relation of muscle, are not explicitly considered. It is currently unclear to what extent low-level dynamics can contribute to the stability of bipedal stance.

In this study, a nonlinear model of the musculoskeletal system incorporating these low-level processes is used to assess the contribution of low-level processes to local stability of the system. As the nonlinear model is smooth in the reference state, linearization at this reference state is possible, and analysis of local stability is straightforward.

Regarding the lowest level, i.e., the force-length-velocity relation of muscle, it has often been suggested (e.g., Hogan 1984; Gottlieb 2000) that cocontraction of antagonistic muscles improves joint impedance and, more specifically, increases the low-frequency joint stiffness, which in turn contributes to the overall stability of the system. In fact, Winter et al. (1998) suggested that this stiffness is sufficient to adequately compensate for the destabilizing gravitational stiffness so that open-loop control could result in a stable system. In the present study, the contribution of the force-length-velocity relation of muscle and, relatedly, cocontraction to the stability of human bipedal stance is the first issue addressed.

Moving up one level in the hierarchy of the system, we next consider the muscle spindle system, a monosynaptic spinal feedback system that is generally viewed as the first neural line of defense against perturbations. Modeling the spindle system as time-delayed negative feedback of contractile element length and velocity, the question is addressed of whether the feedback gains can be chosen such that a locally stable system is obtained. Earlier studies (e.g., He et al. 1991) in which time delays were not taken into account have been criticized because time delays are known to limit the potential contribution of feedback to system impedance. In order to assess how serious this criticism must be taken, we compare the results for the time-delayed system to those for a (hypothetical) nondelayed system.

The neurophysiology of the monosynaptic spindle feedback is such that it can only be negative. This is in line with basic control theory indicating that negative feedback can improve the impedance of an isolated system. However, it is plausible that through a small number of spinal interneurons spindle information can also be fed back positively onto the alpha motoneuron. Furthermore, in a high-dimensional system as considered in this study, it is not necessarily optimal to have negative feedback only. Therefore, we finally consider the question of whether local stability can be improved by allowing positive spindle feedback.

2 Methods

2a Outline of the study

As the independent variables considered in this study do not lend themselves to experimental manipulation, this study is based on modeling only. The model describes the dynamics of the musculoskeletal system during human stance. Input of this forward dynamics model is the neural input of the nine muscle groups modeled. Output of the model is the resulting kinematics and kinetics of the 2D three-segment skeletal model. The local stability of the system is investigated on the basis of a linearization of the system in an almost erect equilibrium posture.

2b Model of the musculoskeletal system

In this study we use an extended version of an existing nonlinear model originally developed to study human vertical jumping (e.g., van Soest and Bobbert 1993) and cycling (van Soest and Casius 2000). One muscle was added to the model as described in van Soest and Casius (2000), resulting in a model having a pair of antagonistic monoarticular muscles at each of the three joints modeled as well as three biarticular muscles (see Fig. 1).

The 2D skeletal model consists of four rigid segments. These segments represent the foot, lower leg, upper leg, and HAT (head, arms, and trunk). The connections between the segments are modeled as frictionless hinge joints between these segments. The foot segment is fixed to the earth. Thus the skeletal model has three mechanical degrees of freedom.

"Muscles" are described by a Hill-type muscle model containing a contractile element, a series elastic element, and a parallel elastic element (see van Soest and Bobbert 1993 for an extensive description). The flow of calculations is schematically represented in Fig. 2. Functions f_1 and f_2 together describe a nonlinear first-order system linking active state q as defined in Ebashi and Endo (1968) to stimulation, the one-dimensional input of the muscle, as proposed by Hatze (1981). In this model of activation dynamics, active state also depends on contractile element length. Function f_3 represents the Hill force-velocity relationship formulated such that contractile element velocity is calculated from contractile element length, force, and active state. This force is calculated in f_5 from series elastic element length, which is modeled as a quadratic spring. Series elastic element length in turn is calculated in f_4 as the difference between muscle-tendon complex length and contractile element

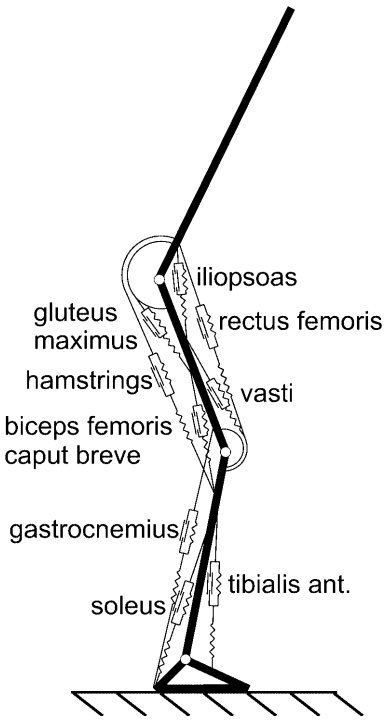

Fig. 1. Schematic representation of the musculoskeletal model used in this study

length. Polynomial relations are used in function f_4 to calculate muscle-tendon complex length from the joint angles; these polynomial relations are based on cadaver studies (Grieve et al. 1978; Huijing, personal communication). Finally, f_6 transforms the muscle forces in their contributions to net joint torques, using moment arms that follow from the same polynomial relations. Together with the gravitational forces these net joint torques determine the acceleration of the skeleton (as well as the reaction forces) in f_7. The Newtonian equations of motion in f_7 are automatically derived using MUSK (Casius 1995). For the complete open-loop system as presented in Fig. 2, the state vector has dimension 24 (three segment angles φ, three segment angular velocities ω, nine Ca^{2+} concentrations γ, and nine contractile element lengths L_{ce}).

All the parameter values of the model are identical to those used in a sprint cycling study (van Soest and Casius 2000). The parameter values for the added muscle (short head of the biceps femoris) were based on Yamaguchi et al. (1990). Values for the most important parameters are presented in Tables 1 and 2.

2c Linearization at a reference equilibrium state

The open-loop controlled musculoskeletal model described above can be formally represented by a nonlinear time-invariant state space model:

$$\begin{aligned} \dot{\boldsymbol{x}} &= \boldsymbol{f}(\boldsymbol{x}, \boldsymbol{stim}) \\ \boldsymbol{y} &= \boldsymbol{g}(\boldsymbol{x}, \boldsymbol{stim}) \end{aligned} \tag{1}$$

where $\boldsymbol{x}$ is the system state vector, $\boldsymbol{stim}$ is the neural input vector, $\boldsymbol{y}$ is the vector of measurable outputs of the system, and $\boldsymbol{f}$ and $\boldsymbol{g}$ are vector functions. Linearization of this open-loop system at any reference point $\boldsymbol{x_0}, \boldsymbol{stim_{ref,0}}$ implies calculation of four matrices of partial derivatives:

$$\begin{aligned} \boldsymbol{\Delta\dot{x}} &= (\partial \boldsymbol{f}/\partial \boldsymbol{x}) \cdot \boldsymbol{\Delta x} + (\partial \boldsymbol{f}/\partial \boldsymbol{stim}) \cdot \boldsymbol{\Delta stim} \\ &= \boldsymbol{A}_{\mathrm{ol}} \cdot \boldsymbol{\Delta x} + \boldsymbol{B}_{\mathrm{ol}} \cdot \boldsymbol{\Delta stim} \\ \boldsymbol{\Delta\dot{y}} &= (\partial \boldsymbol{g}/\partial \dot{\boldsymbol{x}}) \cdot \boldsymbol{\Delta x} + (\partial \boldsymbol{g}/\partial \boldsymbol{stim}) \cdot \boldsymbol{\Delta stim} \\ &= \boldsymbol{C}_{\mathrm{ol}} \cdot \boldsymbol{\Delta x} + \boldsymbol{D}_{\mathrm{ol}} \cdot \boldsymbol{\Delta stim} \end{aligned} \tag{2}$$

The matrices of partial derivatives in Eq. 2 are usually referred to as $\boldsymbol{A}_{\mathrm{ol}}$, $\boldsymbol{B}_{\mathrm{ol}}$, $\boldsymbol{C}_{\mathrm{ol}}$, $\boldsymbol{D}_{\mathrm{ol}}$, $\boldsymbol{A}_{\mathrm{ol}}$ also being referred to as the "system matrix." $\boldsymbol{\Delta}$ in Eq. 2 indicates that the variables are taken relative to the reference point.

Linearization can only be carried out if the partial derivatives in Eq. 2 are well defined. In the musculoskeletal model, there is one relation that violates this smoothness requirement: based on physiological evidence, the slope of the force-velocity curve at the isometric point is different for the concentric and eccentric sides. In order to ensure linearizeability of the model, the eccentric slope was set equal to the concentric one in this study. It was found that this adaptation has a negligible effect on the open-loop dynamics.

In this study, linearization of the model at the various equilibrium states considered was carried out numerically using the central difference method. Care was taken to use the smallest step size for which rounding error was negligible.

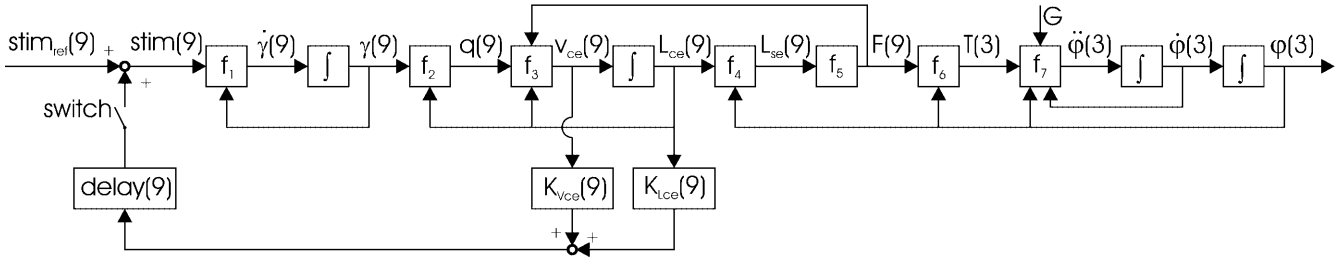

Fig. 2. Block diagram showing the flow of calculations in the nonlinear model. Numbers in parentheses represent the dimension of the juxtaposed variable. Closing the switch transforms the open-loop system into the closed-loop system. Note that in the system with the sign of the feedback as shown, positive values for K_{Vce} and K_{Lce} effectively result in negative feedback. See text for details on blocks f_1 through f_7. Blocks containing the integral sign indicate integration with respect to time

Table 1. Parameter values of the skeletal system. For lower legs and upper legs values are for left and right body side combined. HAT = Head-Arms-Trunk, modeled as one rigid segment. Center of mass (COM) position is relative to the caudal end of the segment. Segment angles are defined counterclockwise from the right horizontal

	Length (m)	COM position (m)	Mass (kg)	Moment of Inertia ($kg \cdot m^2$)	Segment angle (rad)
Lower legs	0.46	0.26	7.1	0.14	1.46
Upper legs	0.49	0.28	16.9	0.42	1.66
HAT	0.90	0.29	55.8	3.90	1.46

Table 2. Muscle parameter values. F_{max} is maximum isometric force, for left and right body side combined; $L_{ce,opt}$ is contractile element optimum length; L_{slack} is series elastic element slack length

	F_{max} (N)	$L_{ce,opt}$ (m)	L_{slack} (m)	Moment arm (m)		
				Ankle	Knee	Hip
Tibialis Ant.	2396	0.087	0.317	−0.037		
Soleus	5991	0.055	0.236	+0.044		
Gastrocnemius	2996	0.055	0.376	+0.044	+0.018	
Vasti	10490	0.093	0.160		−0.042	
Rectus Fem.	3469	0.081	0.340	−0.042	−0.035	
Glutei	5532	0.200	0.150			+0.062
Hamstrings	4426	0.104	0.370		+0.026	+0.077
Iliopsoas	7988	0.102	0.115			−0.050
Biceps C. Breve	1000	0.133	0.100		+0.026	

Regarding the position of the skeletal model in the reference state, the knee and hip joints are chosen to be 0.2 rad from full extension; in this position, the contribution of passive structures can be neglected. The center of gravity is chosen to lie 18% of the foot length in front of the ankle axis. This results in an ankle angle that is in the midrange of the range of motion.

2d Analysis of the local stability of the open-loop system

Local stability of the open-loop controlled system can be directly judged from the properties of the system matrix $\boldsymbol{A}_{ol}$. More precisely, whenever all real parts of the eigenvalues of $\boldsymbol{A}_{ol}$ are negative, the linear system is stable and the underlying nonlinear system is locally stable. Therefore, $MRE(\boldsymbol{A}_{ol})$, which is the maximal real part of the eigenvalues of the system matrix $\boldsymbol{A}_{ol}$, is used as a measure of local stability in this study. For a stable system ($MRE(\boldsymbol{A}_{ol}) < 0$), the negative reciprocal of the value of $MRE(\boldsymbol{A}_{ol})$ indicates the slowest component (that is, the component with the highest time constant) of the system. Another variable related to local stability is the low-frequency joint stiffness, which is an aspect of joint impedance that is easily interpretable. Low-frequency joint stiffness indicates the steady-state net muscle torque change per steady-state joint angle change. If at any of the joints this stabilizing low-frequency joint stiffness does not outweigh the corresponding destabilizing gravitational stiffness, the system cannot be locally stable. In passing, it is noted that the opposite is not true: an adequate low-frequency joint stiffness does not guarantee local stability. The stiffness matrix can be obtained analytically from the linearized system as outlined in the Appendix.

In order to assess the contribution of muscle properties and cocontraction to stability, four systems are compared: (1) a torque-driven system system lacking these muscle properties; (2) a three-muscle system where equilibrium is produced by the monoarticular extensors soleus, vasti, and gluteals; (3) a six-muscle system, where equilibrium is produced through maximal cocontraction of a pair of monoarticular muscles at each joint (soleus and tibialis anterior; vasti and short head of biceps femoris; gluteals and iliopsoas); and (4) the full nine-muscle system, where the nine muscle stimulation levels that minimize $MRE(\boldsymbol{A}_{ol})$ while ensuring that equilibrium is maintained was determined iteratively. In addition to these four systems, the maximally attainable low-frequency stiffness at the required net joint torque was determined for each of the joints separately on the basis of a grid search.

2e Modeling and optimization of muscle spindle feedback and modeling of neural time delays

The firing frequency of muscle spindle afferents is known to depend in a complex way on the length and stretch velocity of the sensory zone (Rothwell 1994). In the present study, a black-box model of spindle feedback is used. It is assumed that the spindle system effectively provides perfect information to the spinal system about contractile element length L_{ce} and velocity v_{ce}. Sensor dynamics is not modeled because its bandwidth far exceeds the range of frequencies that are relevant to postural sway (Rothwell 1994). The analysis is restricted to the monosynaptic loop; that is, spindle information from a muscle feeds back only on the stimulation of that muscle itself; cross couplings between muscles are not considered. As the only issue addressed in this study is local stability, spindle feedback is modeled to be linear. It is assumed that at the spinal level there is full and independent control over the linear feedback gains for length and velocity, for each muscle separately.

Spindle activity does not instantaneously affect stimulation at the neuromuscular junction. The time lag is largely determined by the conduction speed of type Ia and type II afferents and of efferent nerves and is modeled as a pure time delay of 0.035 s (Rothwell 1994). This pure time delay is modeled using a fifth-order Padé filter for each muscle. The structure of the feedback controlled system is shown in Fig. 2 (switch closed). Note in Fig. 2 that, contrary to the customary situation, the sign of the feedback is defined as positive. This is done to ensure that positive feedback gains effectively result in negative feedback.

In terms of the state space model, the muscle spindle feedback controlled system constitutes output feedback

control when the output vector $\Delta \boldsymbol{y}$ in Eq. 2 is defined as the time-delayed $[\Delta \boldsymbol{L}_{ce}; \Delta \boldsymbol{v}_{ce}]$. In other words, the effective input $\Delta \boldsymbol{stim}$ in Eq. 2 can be replaced by:

$$\Delta \boldsymbol{stim} = \Delta \boldsymbol{stim}_{ref} + \boldsymbol{K}_{fb} \cdot \Delta \boldsymbol{y} \tag{3}$$

Here, $\boldsymbol{K}_{fb}$ is a matrix of feedback gains of dimension 9×18, of which 18 elements (9 autogenous length feedback gains and 9 autogenous velocity feedback gains) will be allowed to be nonzero.

After substitution of Eq. 3 in Eq. 2, and using the fact that for our musculoskeletal model $\boldsymbol{D}_{ol}$ is a null matrix, we find:

$$\begin{aligned} \Delta \dot{\boldsymbol{x}} &= (\boldsymbol{A}_{ol} + \boldsymbol{B}_{ol} \cdot \boldsymbol{K}_{fb} \cdot \boldsymbol{C}_{ol}) \cdot \Delta \boldsymbol{x} + \boldsymbol{B}_{ol} \cdot \Delta \boldsymbol{stim}_{ref} \\ &= \boldsymbol{A}_{cl} \cdot \Delta \boldsymbol{x} + \boldsymbol{B}_{ol} \cdot \Delta \boldsymbol{stim}_{ref} \\ \Delta \boldsymbol{y} &= \boldsymbol{C}_{ol} \cdot \Delta \boldsymbol{x} \end{aligned} \tag{4}$$

The matrix $(\boldsymbol{A}_{ol} + B_{ol} \cdot K_{fb} \cdot C_{ol})$ is the system matrix of the closed-loop system and will be referred to as $\boldsymbol{A}_{cl}$. Given the linearized open-loop state space model, $\boldsymbol{A}_{cl}$ is seen to depend on the gain matrix $\boldsymbol{K}_{fb}$ only. Therefore, the question of whether monosynaptic spindle feedback can result in a locally stable system can be addressed by investigating the eigenvalues of $\boldsymbol{A}_{cl}$ as a function of the gain matrix $\boldsymbol{K}_{fb}$. In particular, the aim is to find the gain matrix $\boldsymbol{K}_{fb}$ that minimizes MRE($\boldsymbol{A}_{cl}$). As no analytic methods are available to find the optimal matrix $\boldsymbol{K}_{fb}$, a simulated annealing algorithm for optimization based on Goffe et al. (1994) is used to find the set of feedback gains that minimizes MRE($\boldsymbol{A}_{cl}$). In the optimizations, the feedback gains were allowed to take on values between 0 and 32.

In the study of the contribution of spindle feedback, the position of the skeletal system was identical to that used in the study of cocontraction. Because in reality high levels of cocontraction are not found during human standing, the active state of the nine muscles in the equilibrium position was required to be below 0.25. Cocontraction was chosen such that MRE($\boldsymbol{A}_{cl}$) was minimized while satisfying this constraint on active state.

3 Results

The stability of the open-loop system was investigated for four different situations: (1) torque-control model; (2) three-muscle model; (3) six-muscle model; and (4) nine-muscle model. The resulting MRE($\boldsymbol{A}_{ol}$) and the low-frequency joint stiffnesses are reported in Table 3. Furthermore, the maximally attainable low-frequency joint stiffness at the required net joint torque was found to equal 230, 318, and 791 Nm·rad^{-1} for ankle, knee, and hip, respectively. All in all, it was found that the intrinsic muscle properties contribute to the low-frequency joint stiffness and that cocontraction does so even more strongly; however, it was found impossible to compensate for the destabilizing gravitational stiffness (see Table 3) at the ankle and at the knee. The insufficiency of the low-frequency joint stiffness is reflected in the value of MRE($\boldsymbol{A}_{ol}$), which is positive in all four situations considered, signaling an unstable system. Detailed analysis revealed that the low-frequency joint stiffness originated only partly from the isometric torque-angle relationship of the muscles; it was found that the length dependence of active state that is present in the activation dynamics model described by Hatze (1981) made a substantial contribution to the low-frequency joint stiffness. The instability of the system is confirmed by simulations of the nonlinear model, after an arbitrary perturbation (data not shown).

Table 3. Max(real(eig($\boldsymbol{A}$))) and diagonal elements of the low-frequency joint-stiffness matrix for open-loop torque control (OL_T), and the three-, six-, and nine-muscle open-loop models, and for closed-loop delayed negative (CL_DNF), delayed "arbitrary" (CL_DAF), and nondelayed negative (CL_NNF) feedback control. For comparison, the destabilizing gravitational stiffness at ankle, knee, and hip is also given

	MRE(A) (s^{-1})	Ankle stiffness (Nm·rad^{-1})	Knee stiffness (Nm·rad^{-1})	Hip stiffness (Nm·rad^{-1})
Gravitational stiffness		−811	−469	−159
OL_T	+17.49	0	0	0
OL_3	+7.41	74	35	61
OL_6	+2.85	229	128	361
OL_9	+2.51	172	252	748
CL_DNF	+0.78	1152	760	565
CL_DAF	−0.41	1164	1139	319
CL_NNF	−0.87	1243	814	2170

For the system controlled by time-delayed negative spindle feedback, Fig. 3 presents optimization results for five independent optimization runs each of which started from a random initial guess. Separate optimizations yield values for MRE($\boldsymbol{A}_{cl}$) that are very similar (ranging between +0.78 s^{-1} and +0.79 s^{-1}), while the feedback gains vary somewhat between optimizations. We conclude that local stability cannot be obtained through time-delayed negative spindle feedback. From Table 3 it is noted that the feedback contribution to the low-frequency joint stiffness is such that this stiffness adequately compensates for the destabilizing gravitational stiffness; in other words, the reason for the instability is not that the low-frequency joint stiffness is insufficient.

Figure 3 shows that some of the length gains are zero, suggesting that allowing positive feedback might improve local stability. To follow up on this, five independent optimizations of the feedback gains were carried out where feedback was not required to be negative; this yielded values for MRE($\boldsymbol{A}_{cl}$) ranging from −0.25 s^{-1} to −0.41 s^{-1}, indicating that positive feedback may indeed improve local stability, effectively producing a system that is just barely stable.

Finally, the effect of time delays was assessed by carrying out five optimizations in the absence of time delays (negative feedback). This yielded values for MRE ($\boldsymbol{A}_{cl}$) that ranged from −0.86 s^{-1} to −0.87 s^{-1}, even though there was substantial variation in the underlying feedback gains (data not shown). Comparison to the results for time-delayed negative feedback indicates that

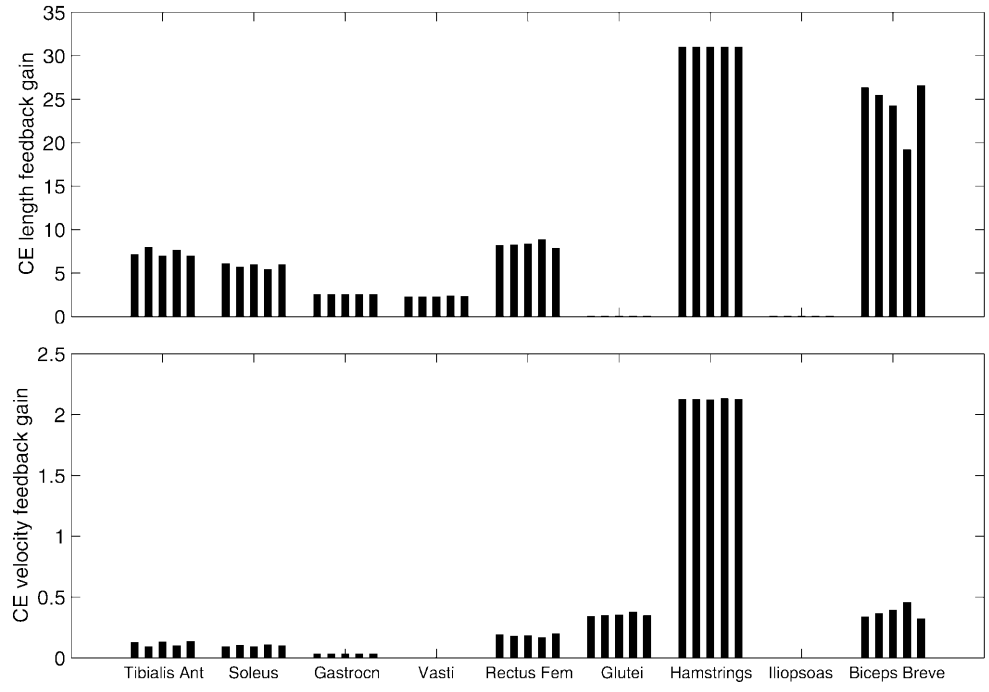

Fig. 3. Results of five independent optimizations of the feedback gains for time-delayed negative feedback of contractile element length and velocity. MRE($\boldsymbol{A}_{\mathrm{cl}}$), the maximum of the real parts of the eigenvalues of the closed-loop system matrix used as the objective function in the optimization, ranges from 0.78 s^{-1} to 0.79 s^{-1}

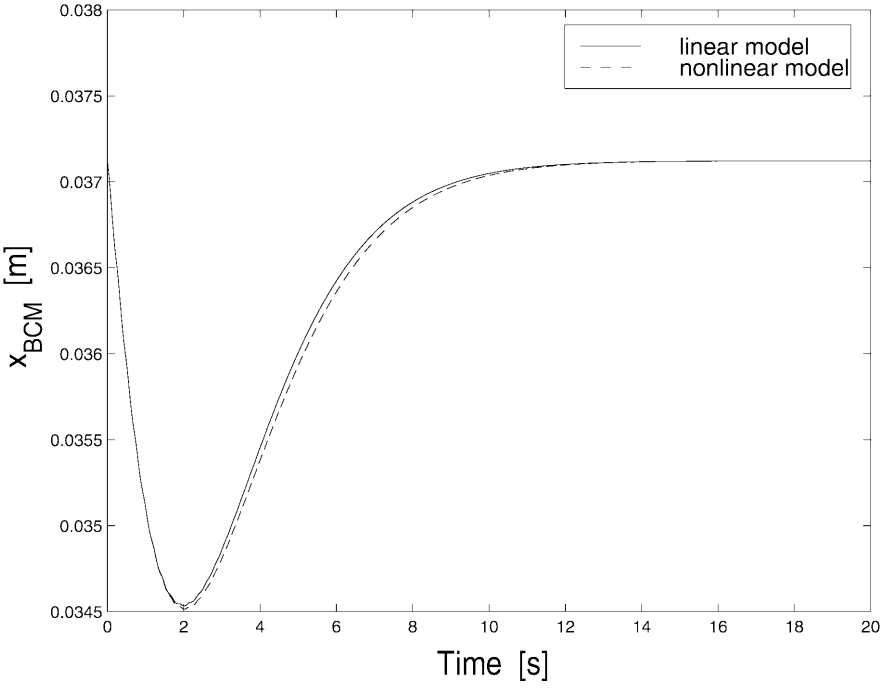

Fig. 4. Comparison of the behavior of the nonlinear and the linearized nondelayed negative feedback controlled system. The horizontal position of the body center of mass (relative to the ankle axis) in response to a 0.01 rad $\cdot s^{-1}$ perturbation of the initial trunk angular velocity is plotted as a function of time

the time delay indeed limits the efficacy of the feedback loop; in the absence of time delays, the contractile element velocity feedback gains were substantially higher. Furthermore, the pattern of the contractile element length feedback gains was different in the absence of time delays, which is reflected in the different pattern of low-frequency joint stiffnesses (see Table 3).

In order to verify that conclusions based on analysis of the linearized system also hold for the nonlinear system, the response of both these systems to an arbitrary perturbation of 0.01 rad $\cdot s^{-1}$ of the trunk angular velocity was calculated (Fig. 4). This comparison was carried out for the (nonrealistic) nondelayed negative feedback system, as this is the system for which MRE($\boldsymbol{A}_{\mathrm{cl}}$) was most negative. It is seen that for small perturbations the responses are very similar, indicating that it is meaningful to analyze the linearized system.

4 Discussion

The first aim of this study was to determine the potential contribution of muscle properties to the local stability of bipedal stance. Next, the contribution of time-delayed

negative muscle spindle feedback was investigated. In addition, the limitations imposed by the time delays were assessed, and the question of whether positive feedback can improve local stability was investigated. It was found that muscle properties improve low-frequency joint stiffness; however, even at maximal cocontraction, open-loop control does not result in a locally stable system. More surprisingly, it was impossible to find negative feedback gains for time-delayed muscle spindle information that yield a locally stable system, for the open loop equilibrium investigated. Lifting the constraint that feedback gains had to be negative did result in a stable system, albeit just barely so. Negative feedback in the absence of the neural time delays did produce a stable system, underlining the limitations imposed by time delays.

Analysis of the open-loop system revealed that muscle properties contribute to low-frequency joint stiffness but do so insufficiently to overcome the destabilizing gravitational stiffness. This finding is not in line with a control scheme for quiet standing proposed by Winter et al. (1998). Given the fact that the model used in this study had been previously shown to reproduce the behavior of human subjects remarkably well in a variety of tasks (e.g., cycling, van Soest and Casius 2000; jumping, van Soest and Bobbert 1993; and lifting, J.C.E. van der Burg et al. 2002, personal communication, submitted), it seems likely that the dynamic properties of the muscles are modeled with reasonable accuracy; consequently, we tend to agree with Morasso and Schieppati (1999) that stable standing cannot be achieved using open-loop control, that is, on the basis of the viscoelastic properties of muscle. These remarks should not be taken to indicate that these properties may as well remain unmodeled. In fact, the difference between the open-loop torque control and the open-loop muscle control (Table 3) shows that the control problem faced by the central nervous system is overestimated when muscle properties remain unmodeled. Furthermore, these muscle properties form the only zero-delay system to counteract perturbations.

It must be noted that in this study, joint stiffness arises from the interaction between the static force-length relations of contractile element and series elastic element of the Hill-type muscle model and from the length-dependence of the active state (Hatze 1981). The contractile element force-length relation is based on myofilament overlap; however, cross-bridge stiffness, which is another aspect of cross-bridge dynamics, is not represented in our Hill-type muscle model. Cross-bridge stiffness is much higher than the stiffness of the static force-length relationship (Zahalak 1990). However, this stiffness is observable primarily during high-frequency vibration experiments (Zahalak 1990); therefore, inclusion of cross-bridge stiffness will not affect the low-frequency stiffness. As open-loop control produced insufficient low-frequency joint stiffness, we expect that our conclusions regarding open-loop control will be upheld when cross-bridge stiffness is modeled. The same reasoning does not necessarily apply to negative spindle feedback control, however, as the low-frequency stiffness is not the cause of instability there. It would be interesting to investigate the contribution to stability of this and other history-dependent aspects of muscle dynamics that are not captured by a Hill-type model.

In modeling spindle feedback, the usual assumption is made that spindle afference signals *contractile element* length and velocity (e.g., Rothwell 1994). It is not always realized that this assumption implies that joint angles and angular velocities are not directly sensed by muscle spindles due to the presence of series elasticity. This may be one factor in explaining why inclusion of negative time-delayed spindle feedback does not yield local stability. Another factor that was directly shown to limit the efficacy of spindle feedback is the presence of neural time delays. The negative effect on stability of the time delays can be readily understood from basic control theory. A third factor that was shown to limit the efficacy of spindle feedback is the assumption that this feedback must be negative. When positive feedback is allowed, a stable system is obtained, even though the time constants are unrealistically large. Given the complexity of the spinal circuitry, it must be expected that positive spindle feedback is a neurophysiological possibility. A final factor that may limit the contribution of spindle feedback as identified in this study concerns the fact that cross couplings of feedback pathways between muscles were not considered. Cross couplings were neglected because they have been shown to be weak in comparison to feedback on the muscle itself (He et al. 1991; Smeets and van der Gon 1993) and because their inclusion would have implied a dramatic increase in the number of feedback gains to be optimized.

In optimizing the spindle feedback gains, sensory dynamics was neglected, sensory noise was not considered, and it was assumed that length and velocity feedback gains could be tuned independently. Despite the fact that length and velocity information is combined at the level of the spindle, the latter assumption is supported by the literature; the sensitivity for length and velocity differs between type Ia and type II spindle afferents, and these sensitivities can be influenced by intrafusal stimulation with static and dynamic gamma efferent fibers (Rothwell 1994). All in all, the assumptions regarding spindle feedback are such that, if anything, this study overestimates the potential contribution of spindle feedback.

In conclusion, optimally tuned time-delayed negative spindle feedback, in combination with the stabilizing properties of muscle, does not suffice to stabilize the musculoskeletal system as modeled in this study. As we are confident that the salient features of the "real" system are adequately represented in this model, it remains an open question what the minimal control requirements are for adequate stability of bipedal standing. In future work we will investigate the potential contribution of low-level force feedback as mediated through Golgi tendon organs.

Acknowledgements. We acknowledge Richard Casius for his help in carrying out the optimizations.

Appendix: Determination of low-frequency joint stiffness

The most straightforward way to obtain low-frequency joint stiffness is to clamp a joint angle at a slightly perturbed value, perform a simulation until steady state has been reached, and take the ratio of the change in joint torque over the change in joint angle. This Appendix deals with the question of how the resulting ratio representing the low-frequency joint stiffness can be directly calculated from the linearized system.

In order to answer this question we want to impose a constant joint angle $\Delta\boldsymbol{\varphi}_{\mathrm{jo,ss}}$ ($_{\mathrm{ss}}$ for steady state) and calculate the steady-state joint torque $\Delta\boldsymbol{\tau}_{\mathrm{ss}}$ that results. We start from the linearized state space model in which we partition the state vector into segment angles $\Delta\boldsymbol{\varphi}$, segment angular velocities $\Delta\boldsymbol{\omega}$, and the muscle-state variables $\Delta\boldsymbol{\mu}$ (actually, contractile element lengths and Ca^{2+} concentrations), and in which we consider only the joint torques $\boldsymbol{\tau}$ as outputs:

$$\begin{bmatrix} \Delta\dot{\boldsymbol{\varphi}} \\ \Delta\dot{\boldsymbol{\omega}} \\ \Delta\dot{\boldsymbol{\mu}} \end{bmatrix} = \begin{bmatrix} \mathbf{0} & \boldsymbol{I} & \mathbf{0} \\ \boldsymbol{A}_{\omega,\varphi} & \boldsymbol{A}_{\omega,\omega} & \boldsymbol{A}_{\omega,\mu} \\ \boldsymbol{A}_{\mu,\varphi} & \boldsymbol{A}_{\mu,\omega} & \boldsymbol{A}_{\mu,\mu} \end{bmatrix} \cdot \begin{bmatrix} \Delta\boldsymbol{\varphi} \\ \Delta\boldsymbol{\omega} \\ \Delta\boldsymbol{\mu} \end{bmatrix} + \boldsymbol{B} \cdot \Delta\boldsymbol{u} \qquad (5)$$

$$\Delta\boldsymbol{\tau} = \begin{bmatrix} \boldsymbol{C}_{\tau,\varphi} & \boldsymbol{C}_{\tau,\omega} & \boldsymbol{C}_{\tau,\mu} \end{bmatrix} \cdot \begin{bmatrix} \Delta\boldsymbol{\varphi} \\ \Delta\boldsymbol{\omega} \\ \Delta\boldsymbol{\mu} \end{bmatrix} \qquad (6)$$

Note that in the context of the present study, $\Delta\boldsymbol{u}$ equals zero at all times because the setpoint is stationary. Then, the steady-state muscle state $\Delta\boldsymbol{\mu}_{\mathrm{ss}}$ that corresponds to a clamped steady-state segment angle vector $\Delta\boldsymbol{\varphi}_{\mathrm{ss}}$ is found from Eq. 5 by setting $\Delta\dot{\boldsymbol{\mu}} = \mathbf{0}$ and noting that a clamped segment angle vector implies that the segment angular velocity vector $\Delta\boldsymbol{\omega} = \mathbf{0}$:

$$\Delta\boldsymbol{\mu}_{\mathrm{ss}} = -\boldsymbol{A}_{\mu,\mu}^{-1} \cdot \boldsymbol{A}_{\mu,\varphi} \cdot \Delta\boldsymbol{\varphi}_{\mathrm{ss}} \qquad (7)$$

Substituting $\Delta\boldsymbol{\varphi} = \Delta\boldsymbol{\varphi}_{\mathrm{ss}}$ and $\Delta\boldsymbol{\mu} = \Delta\boldsymbol{\mu}_{\mathrm{ss}}$ in Eq. 6 and using Eq. 7, we can express the joint torque vector $\Delta\boldsymbol{\tau}_{\mathrm{ss}}$ as a function of the segment angle vector $\Delta\boldsymbol{\varphi}_{\mathrm{ss}}$:

$$\Delta\boldsymbol{\tau}_{\mathrm{ss}} = \left(\boldsymbol{C}_{\tau,\varphi} - \boldsymbol{C}_{\tau,\mu} \cdot \boldsymbol{A}_{\mu,\mu}^{-1} \cdot \boldsymbol{A}_{\mu,\varphi}\right) \cdot \Delta\boldsymbol{\varphi}_{\mathrm{ss}} \qquad (8)$$

As we are interested in the relation between *joint* angle and joint torque, we express the segment angles $\Delta\boldsymbol{\varphi}$ in the joint angles $\Delta\boldsymbol{\varphi}_{\mathrm{jo}}$:

$$\Delta\boldsymbol{\varphi}_{\mathrm{ss}} = \begin{bmatrix} \mathbf{1} & \mathbf{0} & \mathbf{0} \\ \mathbf{1} & \mathbf{1} & \mathbf{0} \\ \mathbf{1} & \mathbf{1} & \mathbf{1} \end{bmatrix} \cdot \Delta\boldsymbol{\varphi}_{\mathrm{jo,ss}} = \boldsymbol{T} \cdot \Delta\boldsymbol{\varphi}_{\mathrm{jo,ss}} \qquad (9)$$

Finally, we substitute Eq. 9 into Eq. 8 and rearrange to obtain the desired expression for the low-frequency joint-stiffness matrix $\boldsymbol{K}_{\mathrm{jo}}$:

$$\begin{aligned} \boldsymbol{K}_{\mathrm{jo}} &= \frac{\partial\boldsymbol{\tau}_{\mathrm{ss}}}{\partial\boldsymbol{\varphi}_{\mathrm{jo,ss}}} \\ &= \left(\boldsymbol{C}_{\tau,\varphi} - \boldsymbol{C}_{\tau,\mu} \cdot \boldsymbol{A}_{\mu,\mu}^{-1} \cdot \boldsymbol{A}_{\mu,\varphi}\right) \cdot \boldsymbol{T} \end{aligned} \qquad (10)$$

References

Bernstein N (1967) The coordination and regulation of movements. Pergamon Press, New York

Casius LJR (1995) MUSK: a software system that supports computer simulations of large scale realistic models of the neuro-musculo-skeletal system. Final report CRG 94.15. Free University, Amsterdam, pp 6–50

Chow CC, Collins JJ (1995) Pinned polymer model of postural control. Phys Rev E 52: 907–912

Chow CC, Lauk M, Collins JJ (1999) The dynamics of quasi-static posture control. Human Mov Sci 18: 725–740

Collins JJ, de Luca CJ (1993) Open-loop and closed-loop control of posture: a random-walk analysis of center-of-pressure trajectories. Exp Brain Res 95: 308–318

Dijkstra TMH (2000) A gentle introduction to the dynamics setpoint model of human postural control during perturbed stance. Human Mov Sci 19: 567–595

Ebashi S, Endo M (1968) Calcium ion and muscular contraction. Prog Biophys Mol Biol 18: 123–183

Eurich CW, Milton JG (1996) Noise-induced transitions in human postural sway. Phys Rev E 54: 6681–6684

Goffe WL, Ferrier GD, Rogers J (1994) Global optimization of statistical functions with simulated annealing. J Econometrics 60: 65–100

Gottlieb GL (2000) Minimizing stress is not enough. Motor Control 4: 64–67

Grieve DW, Pheasant S, Cavanagh PR (1978) Prediction of gastrocnemius length from knee and ankle joint posture. In: Asmussen E, Jørgesen K (eds) Biomechanics VI-A. University Park Press, Baltimore, pp 405–412

Hatze H (1981) Myocybernetic control models of skeletal muscle. University of South Africa, Pretoria, pp 31–42

He J, Levine WS, Loeb GE (1991) Feedback gains for correcting small perturbations to standing posture. IEEE Trans Autom Control 36: 322–332

Hogan N (1984) Adaptive control of mechanical impedance by coactivation of antagonist muscles. IEEE Trans Autom Control AC-29: 681–690

Kuo AD (1995) An optimal control model for analyzing human postural balance. IEEE Trans Biomed Eng 42: 87–101

Lauk M, Chow CC, Pavlik AE, Collins JJ (1998) Human balance out of equilibrium: nonequilibrium statistical mechanics in posture control. Phys Rev Lett 80: 413–416

Loeb GE, Brown IE, Cheng EJ (1999) A hierarchical foundation for models of sensorimotor control. Exp Brain Res 126: 1–18

Morasso PG, Schieppati M (1999) Can muscle stiffness alone stabilize upright standing? J Neurophysiol 83: 1622–1626

Nakata H, Kyonosuke Y (2001) Automatic postural response systems in individuals with congenital total blindness. Gait Posture 14: 36–43

Peterka RJ (2000) Postural control model interpretation of stabilogram diffusion analysis. Biol Cybern 82: 335–343

Rosenblum M, Firsov G, Kuuz R, Pompe B (1998) Human postural control: Force plates experiments and modeling. In: Kanz H et al (eds) Nonlinear analysis of physiological data. Springer, Berlin Heidelberg New York, pp 283–306

Rothwell J (1994) Control of human voluntary movement. Chapman & Hall, London

Smeets JBJ, van der Gon JJD (1993) An unsupervised neural network model for the development of reflex co-ordination. Biol Cybern 70: 417–425

Van der Kooij H, Jacobs R, Koopman B, Grootenboer H (1999) A multisensory integration model of human stance control. Biol Cybern 80: 299–308

Van Soest AJ, Bobbert MF (1993) The contribution of muscle properties in the control of explosive movements. Biol Cybern 69: 195–204

Van Soest AJ, Casius LJR (2000) Which factors determine the optimal pedaling rate in sprint cycling? Med Sci Sports Exerc 32: 1927–34

Winter DA, Patla AE, Prince F, Ishac M, Gielo-Perczak K (1998) Stiffness control of balance in quiet standing. J Neurophysiol 80: 1211–1221

Yamaguchi GT, Sawa AGU, Moran DW, Fessler MJ, Winters JM (1990) A survey of human musculotendon actuator parameters. In: Winters JM, Woo SL-Y (eds) Multiple muscle systems, biomechanics and movement organization. Springer, Berlin Heidelberg New York, pp 717–773

Zahalak GI (1990) Modeling muscle mechanics and energetics. In: Winters JM, Woo SL-Y (eds) Multiple muscle systems: biomechanics and movement organization. Springer, Berlin Heidelberg New York, pp 1–23